nature structural & molecular biology

Structural insight into the substrate specificity of DNA Polymerase μ

Andrea F Moon[1], Miguel Garcia-Diaz[1,2], Katarzyna Bebenek[1,2], Bryan J Davis[3,4], Xuejun Zhong[1,2], Dale A Ramsden[3,4], Thomas A Kunkel[1,2] & Lars C Pedersen[1]

DNA polymerase μ (Pol μ) is a family X enzyme with unique substrate specificity that contributes to its specialized role in nonhomologous DNA end joining (NHEJ). To investigate Pol μ's unusual substrate specificity, we describe the 2.4 Å crystal structure of the polymerase domain of murine Pol μ bound to gapped DNA with a correct dNTP at the active site. This structure reveals substrate interactions with side chains in Pol μ that differ from other family X members. For example, a single amino acid substitution, H329A, has little effect on template-dependent synthesis by Pol μ from a paired primer terminus, but it reduces both template-independent and template-dependent synthesis during NHEJ of intermediates whose 3′ ends lack complementary template strand nucleotides. These results provide insight into the substrate specificity and differing functions of four closely related mammalian family X DNA polymerases.

To accomplish the many DNA transactions involved in stably maintaining and replicating large genomes, mammals encode 16 DNA polymerases classified in families A, B, X and Y[1]. Clues to their functions include their substrate specificity, which can differ substantially, even for members of the same family. For example, two family X enzymes with intrinsic 5′-deoxyribose 5′-phosphate (dRP) lyase activities, DNA polymerase β (Pol β) and Pol λ, are template dependent and efficiently fill short gaps, consistent with synthesis during short patch base excision repair[2,3]. Unlike Pol β, Pol λ has a BRCT domain and probably participates in NHEJ of double-strand breaks (DSBs) in DNA[4–6]. Specifically, Pol λ has a role in V(D)J recombination at immunoglobulin heavy-chain loci[7,8]. Two other family X members are associated with V(D)J recombination. Terminal deoxyribonucleotidyl transferase (TdT) is a template-independent DNA polymerase[9] that synthesizes N regions (stretches of randomly added nucleotides) at junctions of immunoglobulin genes during V(D)J recombination[10]. The other is Pol μ, which promotes accurate immunoglobulin κ light-chain recombination[11].

Pol μ has an unusual primer-template specificity. Like Pol β and Pol λ, Pol μ can fill short gaps in a template-dependent manner[12], yet it also shares with TdT the ability to catalyze template-independent synthesis[13]. Pol μ has an unusually high capacity to extend misaligned primer termini[14]; it can perform translesion synthesis (TLS) *in vitro*[15,16] and it discriminates against incorporating ribonucleoside triphosphates to a lesser extent than do Pol β and Pol λ[17,18]. When Pol μ functions with Ku, XRCC4 and DNA ligase IV to repair DSBs by NHEJ, it fills short gaps in a template-dependent manner by extending primer termini lacking one or two complementary template strand nucleotides, a property not shared by Pol λ[6]. Thus Pol β, Pol λ, Pol μ and TdT show a gradient of template dependency, and among Pol λ, Pol μ and TdT, the enzyme used during NHEJ may partly be determined by the nature of the ends to be joined.

To test the relationship between substrate specificity and physiological function, one can compare structures of these polymerases bound to primer-templates. Structures already exist for Pol β[19–22], Pol λ[23–26] and TdT[27], but not yet for Pol μ. Here we fill this knowledge gap by describing a 2.4-Å crystal structure of a ternary complex of the polymerase domain of murine Pol μ. This structure reveals substrate interactions unique to Pol μ, compared with Pol β, Pol λ and TdT. To test whether such differences are important for unusual substrate use by Pol μ, we examined the properties of the wild-type enzyme and an H329A mutant that perturbs interactions with the DNA that are not found in Pol β and Pol λ. A similar substitution was performed on the homologous histidine (H342A) in human TdT. These mutations were made to test whether the histidine is important for template-independent synthesis and for template-dependent synthesis with substrates lacking a template nucleotide at the 3′ primer terminus.

RESULTS

Overall structure of a ternary Pol μ–DNA–ddTTP complex

The polymerization domain (Pro132–Ala496) of murine Pol μ was crystallized in a ternary complex with a gapped template-primer and a correctly paired nucleoside triphosphate bound in the nascent base pair–binding pocket. The DNA contained an 11-nucleotide (nt)

[1]Laboratory of Structural Biology and [2]Laboratory of Molecular Genetics, National Institute of Environmental Health Sciences (National Institutes of Health, US Department of Health and Human Services), 111 T.W. Alexander Drive, MD F3-09, Research Triangle Park, North Carolina 27709, USA. [3]Department of Biochemistry and Biophysics and [4]Curriculum in Genetics and Molecular Biology, 32-0444 Lineberger Comprehensive Cancer Center, University of North Carolina at Chapel Hill, Chapel Hill, North Carolina 27599, USA. Correspondence should be addressed to T.A.K. (kunkel@niehs.nih.gov).

Received 2 August; accepted 10 November; published online 10 December 2006; corrected after print 15 June 2007; doi:10.1038/nsmb1180

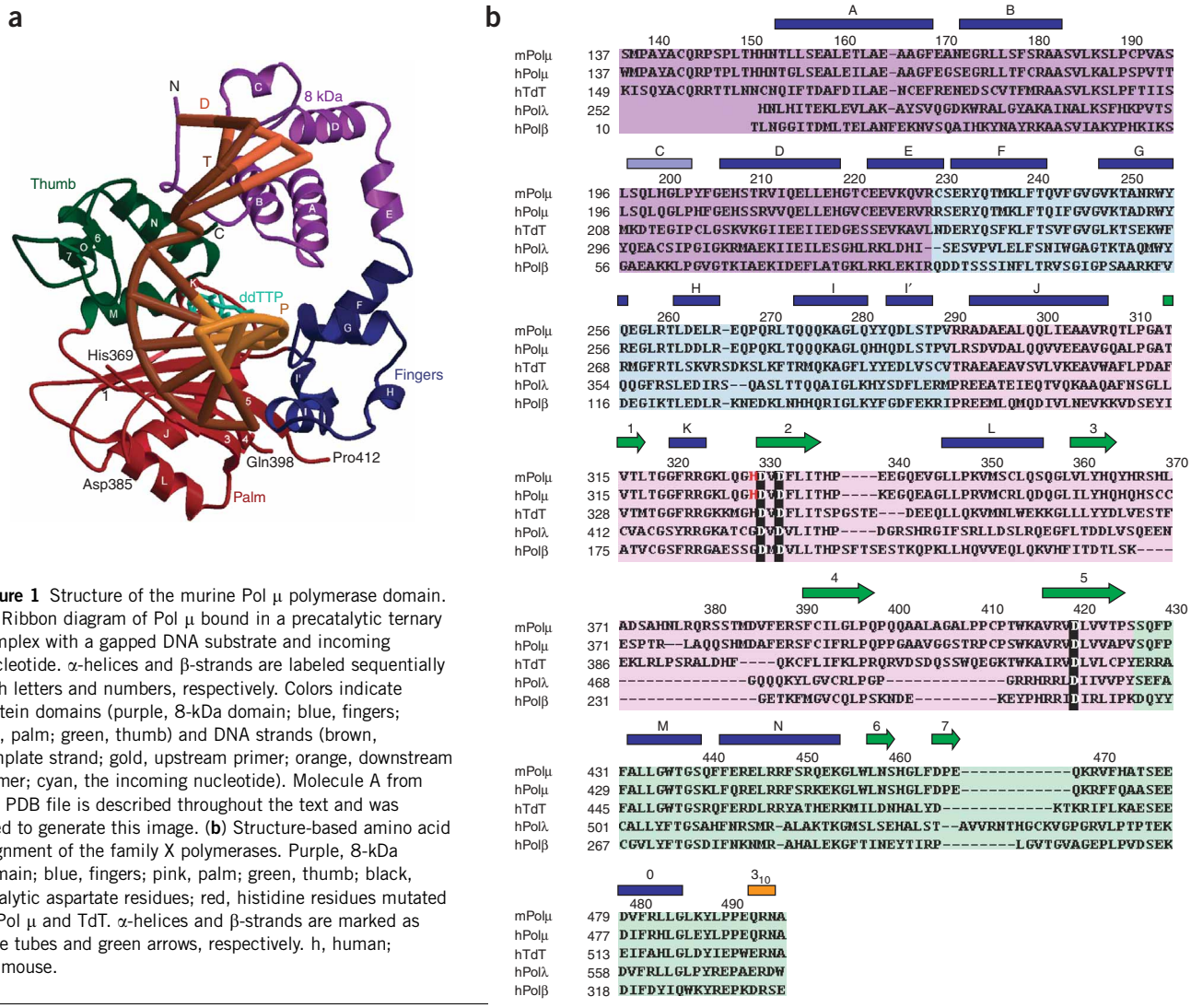

Figure 1 Structure of the murine Pol μ polymerase domain. (**a**) Ribbon diagram of Pol μ bound in a precatalytic ternary complex with a gapped DNA substrate and incoming nucleotide. α-helices and β-strands are labeled sequentially with letters and numbers, respectively. Colors indicate protein domains (purple, 8-kDa domain; blue, fingers; red, palm; green, thumb) and DNA strands (brown, template strand; gold, upstream primer; orange, downstream primer; cyan, the incoming nucleotide). Molecule A from the PDB file is described throughout the text and was used to generate this image. (**b**) Structure-based amino acid alignment of the family X polymerases. Purple, 8-kDa domain; blue, fingers; pink, palm; green, thumb; black, catalytic aspartate residues; red, histidine residues mutated in Pol μ and TdT. α-helices and β-strands are marked as blue tubes and green arrows, respectively. h, human; m, mouse.

template, a 5-nt upstream primer and a 5′-phosphorylated 4-nt downstream primer, generating a 2-nt gapped substrate. Adding ddTTP allowed incorporation of one nucleotide onto the primer and binding of incoming nucleotide, creating a precatalytic ternary complex (**Fig. 1a**). Crystals of this ternary complex diffract to 2.4-Å resolution and contain two molecules of Pol μ (designated A and B), each with bound substrate. The overall fold of Pol μ is characteristic of other family X polymerases (**Fig. 1b**), consisting of the fingers (Val228–Thr288), palm (Pro289–Thr424) and thumb (Pro425–Ala496) subdomains and an N-terminal 8-kDa domain (Leu149–Gln227). A summary of the interactions between protein domains and the bound DNA is diagrammed in **Figure 2**.

In this ternary complex, Pol μ is in the closed conformation characteristic of other family X polymerases[22,24,27]. The Cα backbone of Pol μ superimposes with those of Pol β (PDB entry 1BPY), Pol λ (PDB entry 1XSN), and TdT (PDB entry 1JMS) with r.m.s. deviations of 2.036 Å (over 278 Cα atoms), 1.703 Å (over 277 Cα atoms) and 1.326 Å (over 318 Cα atoms), respectively. Pol μ differs from other family X enzymes with respect to several loop regions interspersed between conserved secondary structural elements. This includes a loop between β-strand 7 and α-helix O in the thumb domain (Asp465–Val471; **Fig. 3a**) and a longer loop with 17 residues (His366–Arg389; **Fig. 3b**).

Protein-DNA interactions

The template strand in the Pol μ ternary complex is bent 90°, exposing the unpaired template base for pairing with the incoming nucleotide. The two molecules of Pol μ in the asymmetric unit (A and B) have similar overall folds (r.m.s. of 0.805 Å over 324 Cα atoms). Interactions of Pol μ residues with the DNA (**Fig. 2**) involve all subdomains of the catalytic core but differ somewhat from those of either Pol β or Pol λ[24]. In Pol λ, protein contacts with the template strand involve multiple putative nonbonded and hydrogen-bonding interactions from the thumb subdomain to the templating nucleotide and the template nucleotide opposite the primer terminus (numbered T5-T6). In Pol μ, there are only two putative hydrogen-bonding interactions from the fingers subdomain to the template strand (both to T11), one of which is mediated by a bridging water molecule (water HOH128). There are extensive nonbonded and hydrogen-bonding interactions from the palm subdomain to the upstream region of the template strand (T8–T11), mostly in a pocket formed by Pol μ residues His366–His369. Thus, there is a high density of interactions along the upstream template region and another surrounding the templating nucleotide. In contrast to Pol λ, there are fewer Pol μ interactions with nucleotides (T6 and T7).

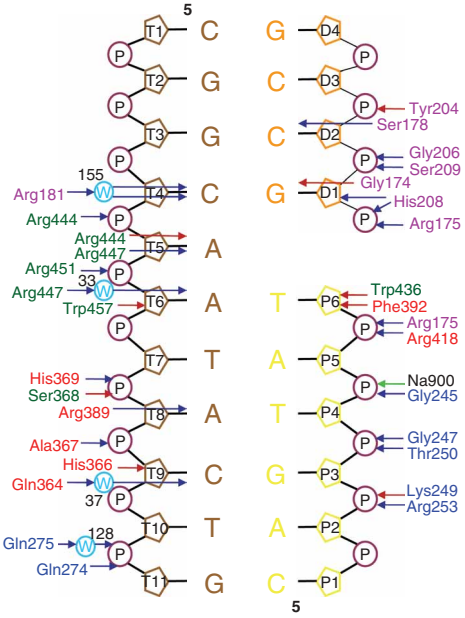

Figure 2 Interactions between Pol μ and the gapped primer-template duplex, shown in a stick diagram, colored as in **Figure 1**. Blue arrows, hydrogen bonds (≤3.2 Å); red arrows, nonbonded interactions; W, water molecules mediating protein-DNA interactions; P, DNA backbone phosphates. DNA residue numbers are shown inside pentagons representing ribose sugars.

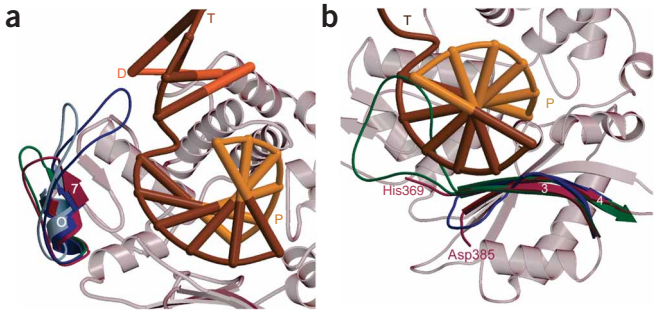

Figure 3 Comparison of loop conformations between mammalian family X polymerases. (**a**) Comparison of the loop between β-strand 7 and α-helix O in all family X polymerases. Maroon, Pol μ; green, TdT; blue-gray, Pol β; dark blue, Pol λ. This loop is the site of protein-protein interaction of Pol β with the DNA-repair protein XRCC1. Also shown is the rest of Pol μ (light gray) and DNA strands colored as in **Figure 1**. (**b**) Comparison of the loop between β-strands 3 and 4 in all mammalian family X polymerases, colored as in **a**. The equivalent region in Pol β is small enough to be described as a turn and is not shown in this figure in the interest of clarity. The position and length of this loop are proposed to have a role in template-independent synthesis by TdT.

Analysis of the electrostatic surface of Pol μ (**Fig. 4a**) indicates that the template strand lies in a slightly positively charged groove along the protein surface. The groove occupied by the upstream primer has a higher concentration of positively charged residues and therefore may be more tightly bound. An interaction common to Pol μ and Pol λ is stacking of the templating base (T5) with an arginine, Arg444 in Pol μ and Arg514 in Pol λ[24]. The equivalent residue in Pol β is a lysine residue (Lys280) with a similar function. Notably absent in Pol μ is a stacking interaction between the base (T4) upstream of the templating base and His34 in Pol β or Trp274 in Pol λ. A glycine residue is found at this position in Pol μ (Gly174, **Fig. 1b**).

Interactions between the protein and the downstream primer are mediated by the 8-kDa domain, specifically by a helix-hairpin-helix motif (HhH; α helices C and D, residues Leu196–Leu216; **Fig. 1**). In Pol μ, as in TdT, α-helix C is distorted compared with the more canonical helix in Pol β and Pol λ, most probably because of the sequence of the hairpin region, which is HϕG rather than GϕG (where ϕ is a hydrophobic residue)[27]. Most interactions involving the first HhH are putative hydrogen-bonding interactions, and most are directed to the phosphate backbone of the primer (**Fig. 2**). The 5′-phosphate of the downstream primer is recognized and bound by the 8-kDa domain (**Fig. 4a**). There are two putative hydrogen bonds with the 5′-phosphate, through Arg175 (NE, according to the nomenclature of the Protein Data Bank) and His208 (ND1; **Fig. 4b**), but the binding pocket for the 5′-phosphate (**Fig. 4c**) is not as positively charged as in Pol β and Pol λ.

The palm and fingers mediate interactions with the upstream primer (**Fig. 2**) that are more numerous and span a larger region than those found in Pol λ. The phosphate backbone of primer nucleotides P3-P4 is nestled in a pocket created by protein residues Gly247–Thr250 and is positioned by both nonbonded and hydrogen-bonding interactions. The motif responsible for these interactions is the second HhH motif[28] within the fingers (α helices F and G, Arg233–Gln256). These interactions may allow the protein to align the primer within the DNA-binding cleft, whereas interactions between the palm subdomain and primer terminus are crucial for correctly positioning that nucleotide for catalysis. As with Pol λ,

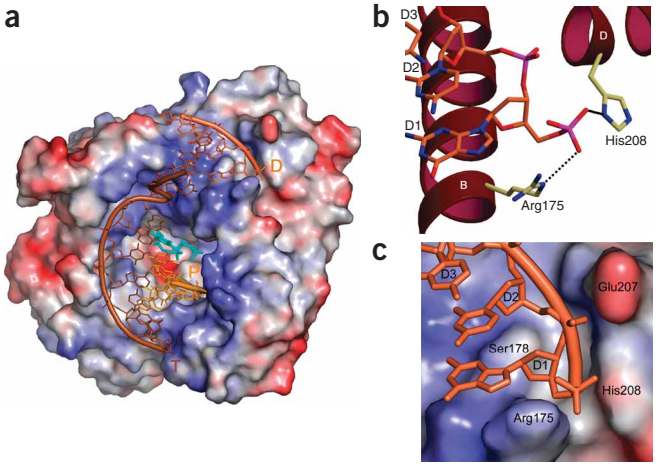

Figure 4 Electrostatic interactions between Pol μ and the bound DNA. (**a**) Electrostatic surface plot of Pol μ. Potential plot was calculated using the Adaptive Poisson-Boltzmann Solver tool in PyMOL. The potential ranges from –8 kT e^{-1} (red) to 8 kT e^{-1} (blue). The bound DNA molecule is shown, colored as in **Figure 1**. The incoming nucleotide (cyan) is bound in a positively charged channel in the center of the figure. (**b**) Interactions with the 5′-phosphate on the downstream primer. Secondary structural elements of Pol μ are shown as labeled maroon ribbons. Dotted line represents putative hydrogen bonds between Arg175 and His208 of Pol μ and the 5′-phosphate. DNA residues in the downstream primer are labeled in black. (**c**) Electrostatic surface plot (as in **b**) of the 5′-phosphate–binding pocket in Pol μ. Downstream primer of bound DNA duplex is shown as orange sticks, with the coil of the phosphate backbone connecting the residues.

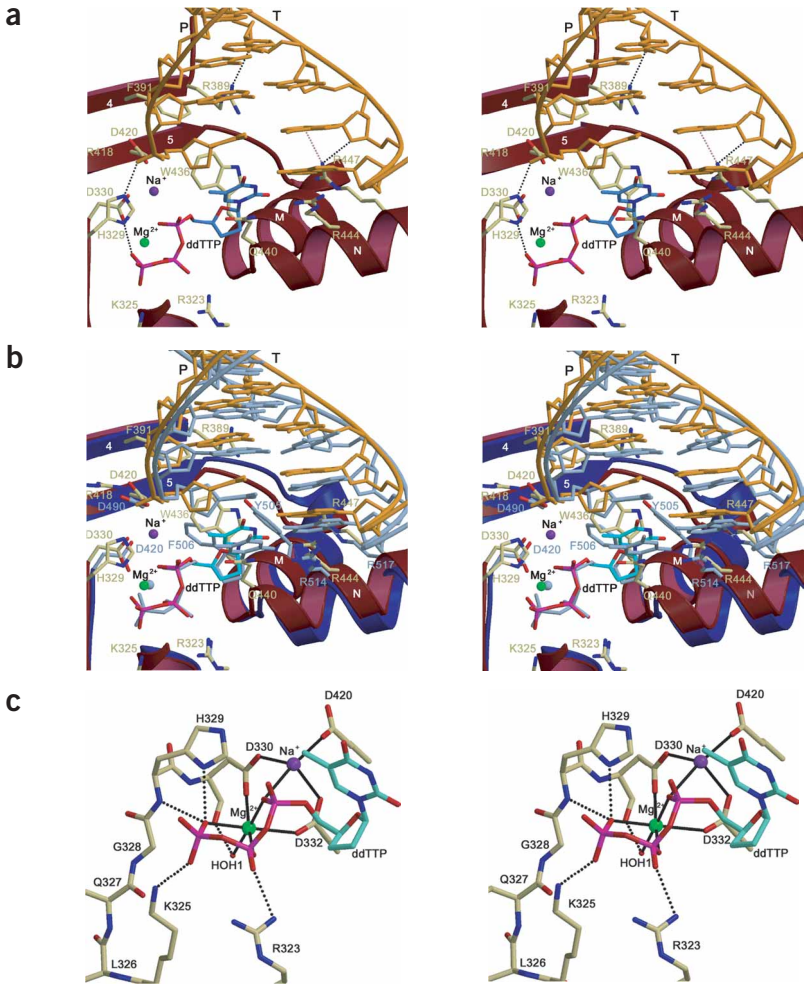

Figure 5 The active site of Pol μ. (**a**) Stereo view of active site organization in Pol μ. Maroon, structural elements of Pol μ; orange DNA strands associated with the ternary complex (T, template; P, upstream primer); tan sticks, side chains of protein residues (numbered); cyan, the incoming nucleotide; green sphere, Mg^{2+}; purple sphere, Na^{+}; black dotted lines, putative hydrogen bonds; pink dotted lines, hydrogen bonds mediated by water molecules. (**b**) Comparison in stereo view of Pol μ and Pol λ active site residues. Maroon ribbon and tan sticks, Pol μ (with associated DNA in orange and incoming nucleotide in cyan); dark blue ribbon and blue-gray sticks, Pol λ (with associated DNA and incoming nucleotide in blue-gray). (**c**) Stereo view of interactions with the incoming nucleotide. Dotted lines, putative hydrogen bonds between protein residues and the nucleotide (cyan); solid lines, interactions that serve to coordinate Mg^{+2} (green) or Na^{+} (purple).

most interactions between Pol μ and the upstream duplex are with the phosphate backbone. The exception is Arg389, located in the minor groove, whose NH2 atom is approximately 3.17 Å from the O4′ position on the T8 ribose (**Fig. 5a**). Also notable is that the position of the primer terminal nucleotide appears to be regulated by two putative hydrogen bonds to its 5′-phosphate, involving His329 NE2 and Arg418 NE. In addition, the position of the ribose sugar is influenced by interactions with the side chains of Trp436 and Phe391 (**Fig. 5a**).

Minor groove interactions

Interactions of side chains of certain polymerases with the minor groove of the primer-template at and upstream of the active site are important for processivity and fidelity of polymerization[24,29–31]. Pol μ has a few minor groove interactions, some of which are mediated by bridging water molecules (**Fig. 5a**). These include an interaction between Arg447 NH1 and the N3 position of the templating base, equivalent to those of Arg517 in Pol λ and Arg283 in Pol β (**Fig. 5a**). Arg447 also interacts with the N3 position of T6, mediated by a water molecule (HOH33). A similar interaction is seen between Arg181 NH2 and either the O2 or O4′ position of T4, bridged by the HOH155 water. Additional minor groove interactions include Arg389 NH2 with the O4′ of T8 and Ser178 OG with the O4′ of D2 (**Fig. 2**).

Notably lacking is conservation of the Tyr-Phe motif seen in Pol λ (Tyr505-Phe506) and Pol β (Tyr271-Phe272). These residues participate in concerted movement upon binding of the incoming nucleotide, resulting in minor groove interactions with the base on the primer terminus and correct positioning of the primer terminus for catalysis[24]. The Tyr-Phe motif is also thought to select for binding of deoxyribo- over ribonucleotides[30]. In Pol μ, the residues in this motif are replaced by Gly435 and Trp436 (**Fig. 5a**,**b**). Gly435 alone is largely responsible for Pol μ's ability to accommodate ribonucleotides, as mutation of Gly435 to tyrosine nearly eliminated binding of ribonucleotides. Subsequent mutation of Trp436 to phenylalanine did not produce the same preference for deoxyribonucleotides. In addition, the dual mutation G435Y W436F produces a protein with greatly diminished catalytic activity[18]. Therefore, despite the lack of conservation of the Tyr-Phe motif, these two residues clearly have an important role in Pol μ activity.

Active-site conformation

Many interactions between Pol μ and the incoming nucleotide are similar to those observed with Pol β and Pol λ[24,32]. The incoming triphosphate is coordinated with a Mg^{+2} ion, which aids in correctly positioning the nucleotide within the active site (**Fig. 5b**,**c**). A second metal helps position the 3′-hydroxyl on the primer terminus to attack the α-phosphate of the incoming nucleotide[32,33]. In the Pol μ structure, the nucleotide-binding Mg^{+2} ion is present, but because of the absence of the 3′-hydroxyl on the primer terminus, a Na^{+} ion occupies the catalytic metal site with low occupancy. There are several putative hydrogen-bonding interactions between active-site residues and the triphosphate oxygen atoms (**Fig. 5c**) and a possible hydrogen bond from the β-phosphate oxygen O2B to the side chain of Arg323 (NH2, 2.89 Å). All residues participating in these interactions are conserved in family X polymerases (**Fig. 1b**). There are two putative interactions with the γ-phosphate oxygens. The first is from O1G to Lys325 (NZ, 2.83 Å), which is conserved in Pol λ, Pol μ and TdT, but not in Pol β, which has an alanine at that position. The second putative hydrogen bond with the γ-phosphate is between O3G and His329 (ND1, 2.93 Å). This residue is conserved between Pol μ

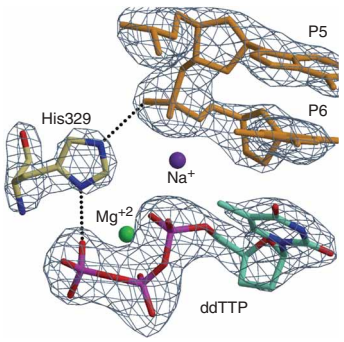

Figure 6 Role of Pol μ H329A in catalysis by Pol μ. Shown are interactions of His329 with the primer terminus and the incoming nucleotide. Tan sticks, His329; gold sticks, residues in the primer strand; cyan sticks, incoming ddTTP; purple sphere, Na^{+}; green sphere, Mg^{+2}; blue-gray mesh, simulated annealing $F_o - F_c$ omit electron density map contoured at 2.5 σ; dotted lines, putative hydrogen bonds between His329 and the primer terminus or the incoming nucleotide.

and TdT, but a glycine is at this position in Pol β and Pol λ (**Fig. 1b** and **Fig. 5b**).

His329 and NHEJ substrate specificity requirements

Catalysis by a DNA polymerase requires precise positioning of the primer and incoming dNTP. This is mainly achieved through protein-DNA interactions that are sensitive to the conformations of all substrates involved in the reaction, including the primer and template strands and the incoming dNTP. Synthesis performed by TdT and Pol μ deviates from canonical polymerization reactions in that key structural substrate elements critical for other polymerases to achieve catalysis can be missing in TdT and Pol μ. It follows that, in these reactions, proper geometric alignment of the substrates has to be achieved irrespective of the conformation (or presence) of the template strand. The Pol μ His329 side chain is positioned such that it could hydrogen-bond to the phosphate of the primer-terminal residue and the γ-phosphate of the incoming dNTP (**Fig. 5a** and **Fig. 6**). Thus, this residue aids in circumventing the absence of the template residues that would normally help position the primer terminus and the incoming dNTP, thereby enabling the unique reactions of which TdT and Pol μ are capable.

To test this hypothesis, we substituted alanine for this histidine in full-length human Pol μ (H329A) and in full-length TdT (H342A). We

Table 1 Steady-state kinetic analysis of nucleotide incorporation

Gap-filling synthesis on dsDNA gapped substrate

Enzyme	k_{cat} (s^{-1})	K_m (μM)	k_{cat}/K_m (s^{-1} μM^{-1})
Wild-type human Pol μ	0.047 ± 0.024	11 ± 4.7	(4.3 ± 0.87) × 10^{-3}
Human Pol μ H329A	0.015 ± 0.007	6.0 ± 3.2	(2.8 ± 0.8) × 10^{-3}

Synthesis on ssDNA substrate

Enzyme	k_{cat} (s^{-1})	K_m (μM)	k_{cat}/K_m ($s^{-1}\mu M^{-1}$)
Wild-type human Pol μ	(2.8 ± 0.9) × 10^{-3}	83 ± 38	(43 ± 29) × 10^{-6}
Human Pol μ H329A	Not detected	Not detected	–

Errors shown are s.d.

first examined the steady-state kinetic parameters for Pol μ during template-dependent synthesis on a gapped dsDNA substrate. Pol μ H329A remained proficient, showing only mildly reduced activity relative to wild-type (**Table 1** and **Fig. 7a**). This is consistent with a relatively minor role for this residue in canonical polymerization reactions. Pol μ and TdT are both active for template-independent incorporation onto a ssDNA primer and, with substantially lower efficiency, onto a blunt-ended duplex. Template-independent activity on ssDNA was reduced approximately 40-fold with the Pol μ H329A mutant (relative to wild-type Pol μ) and approximately 100-fold with the TdT H342A mutant (relative to wild-type TdT; **Fig. 7b,c**). Alanine substitutions in both enzymes also strongly reduced template-independent incorporation onto duplex substrates with 3′ overhangs of 1, 3 and 5 nt (data not shown). Thus, the conserved histidine residue appears to stabilize the primer terminus and the incoming nucleotide (**Fig. 5a** and **Fig. 6**), apparently having a minimal role in the presence of template strand interactions but becoming crucial when these interactions are absent.

Pol μ has been implicated in template-dependent gap-filling repair of DSBs by NHEJ[12]. This includes the unique ability of Pol μ to catalyze template-dependent synthesis in the absence of a template strand nucleotide opposite the primer terminus[6]. By virtue of its interactions with the primer terminus and the incoming dNTP (**Fig. 5a** and **Fig. 6**), His329 could contribute to this unique activity. This histidine may thus be required whenever the primer terminus and incoming nucleotide cannot be aligned by base-pairing with a template, whether the nucleotide is added 'randomly', as for TdT

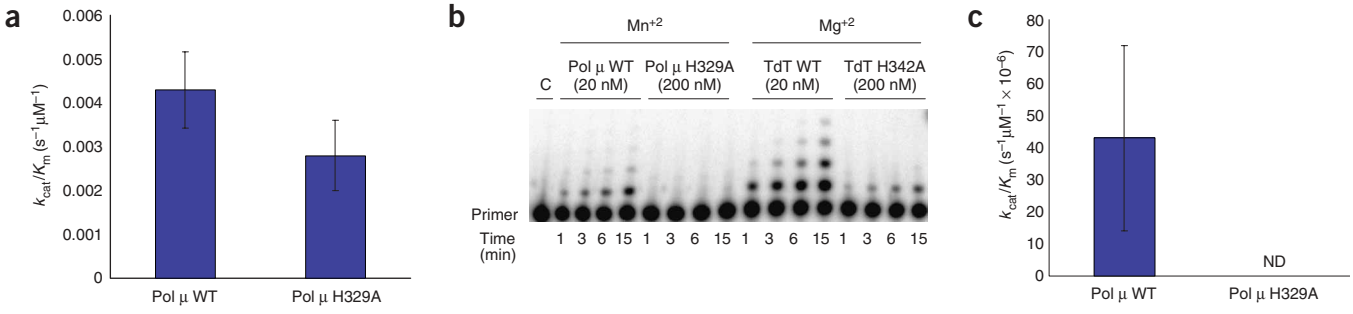

Figure 7 Analysis of catalytic activity for Pol μ and TdT. (**a**) Catalytic efficiency of wild-type and H329A mutant Pol μ on gapped dsDNA substrate. Catalytic efficiency values were calculated by dividing the catalytic rate by the K_m. Error bars represent s.d. (**b**) Template-independent synthesis by Pol μ and TdT. Reactions were performed as described in Methods, using ssDNA, dNTPs, $MnCl_2$ (Pol μ) or $MgCl_2$ (TdT), and either wild-type Pol μ or TdT or the His→Ala mutant. Control reaction (C) contained no polymerase. Aliquots of the reaction mixture were removed after 1, 3, 6 and 15 min, and products were resolved using 12% PAGE. (**c**) Catalytic efficiency of wild-type and H329A mutant Pol μ with ssDNA. ND, not detectable.

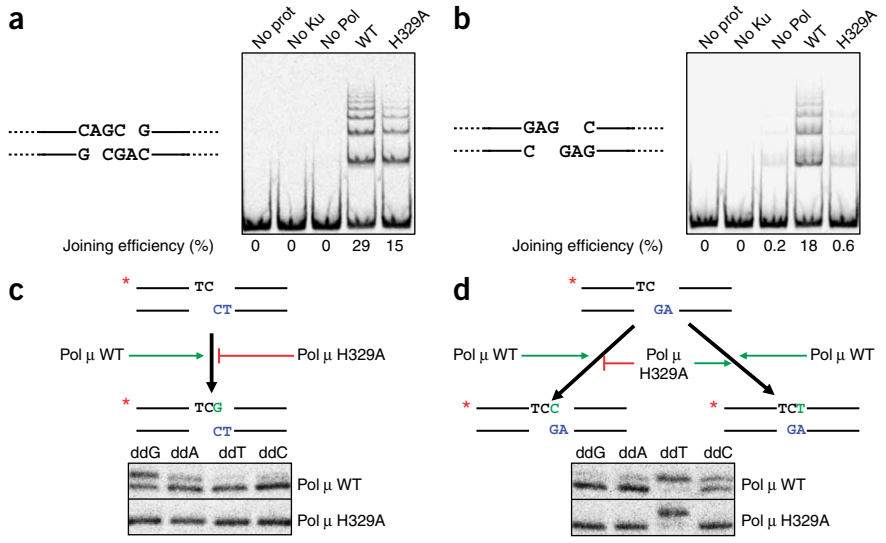

Figure 8 Role of Pol μ His329 in template-dependent synthesis during nonhomologous end-joining. (**a**,**b**) NHEJ assays on DSB substrate with either two (**a**) or no complementary nucleotides (**b**). End structure of each 300-bp DNA substrate is depicted at left; spaces in DNA sequence indicate synthesis required for joining. End-joining efficiencies (see Methods) are noted below gel lanes. (**c**,**d**) Synthesis in the absence of joining. Substrates were labeled DNA with a TC 3′ overhang mixed with unlabeled DNA with either a TC 3′ overhang (**c**) or an AG 3′ overhang (**d**). End structures of the 300-bp DNA substrates used for the proposed template-dependent synthesis activities are depicted; red asterisk marks labeled primer strand.

(**Fig. 7b**), or in a mostly template-dependent manner using a template from another DNA end, as for Pol μ in the context of NHEJ[6]. Therefore, we tested the impact of the H329A mutant in the context of NHEJ of two different types of DNA ends in the presence of Ku, XRCC4 and DNA ligase IV. Mutation of His329 to alanine in Pol μ had little impact on nucleotide incorporation with a NHEJ substrate where alignment of ends is assisted by base-pairing, as the activity of H329A was reduced only two-fold relative to wild-type (**Fig. 8a**), in agreement with kinetic analysis of template-dependent synthesis (**Table 1**). In contrast, when the substrate lacked complementary base pairs at the ends (**Fig. 8b**), the H329A mutant was 30-fold less active than wild-type Pol μ.

The reduced activity of Pol μ H329A in the latter context is thus seemingly linked to its inability to perform template-independent synthesis. However, we have previously suggested that Pol μ remains mostly template dependent in this context[6]. To better establish the template-dependent nature of synthesis by Pol μ in NHEJ, we also compared the ability of wild-type and H329A mutant Pol μ to incorporate each of the four individual ddNTPs in two different NHEJ reactions. Both used a common radiolabeled TC 3′ overhang ('primer'). Synthesis from this overhang was measured in the presence of a ten-fold excess of an unlabeled NHEJ 'template' with the same TC 3′ overhang (**Fig. 8c**, top), or with an AG 3′ overhang (**Fig. 8d**, top). Wild-type Pol μ, but not the H329A mutant, efficiently incorporated ddGMP when using the template with the TC 3′ overhang (**Fig. 8c**, bottom), and it efficiently incorporated complementary ddCMP when using the template with an AG 3′ overhang. Neither of these two correct incorporation reactions occurred with the H329A mutant (**Fig. 8c**,**d**, bottom). Nonetheless, the H329A mutant retained robust activity for incorporation of ddTTP using the template with an AG 3′ overhang (**Fig. 8d**, bottom), consistent with retention of the ability to extend a primer terminus containing one correct base pair at the terminus (**Fig. 8d**, top left substrate).

DISCUSSION

With this report, structures are now available for all four mammalian family X DNA polymerases. A comparison of these structures reveals that Pol μ differs from other family X enzymes in several notable ways. This includes differences in several loop regions that are not mediating crystal contacts and thus may be biologically relevant. For example, the loop between β-strand 7 and α-helix O in the thumb domain greatly varies among Pol β (Arg299–Leu311), Pol λ (Thr534–Leu551) and Pol μ (Asp465–Val471) (**Fig. 3a**). In Pol λ, there is a short β-strand (β-strand 8) between β-strand 7 and α-helix O that is not present in Pol β or Pol μ. This loop in Pol λ is suggested to stabilize the extrahelical nucleotide present in frame-shift intermediates[26]. In Pol β, this loop has been found to have an important role in interactions with repair proteins[34]. In Pol μ, this loop is much shorter than in Pol λ or Pol β and positioned farther from the binding cleft, a conformation similar to that found in TdT. Such conformational differences may prove to be important, possibly affecting interactions with DNA or protein binding factors. Another difference is in the loop between β-strands 3 and 4 (Loop I)[6,23,27]. The length and conformation of this loop is thought to affect template dependence among the family X polymerases[6,27]. Loop I, small enough in Pol β to be described as a turn (Gly231–Thr233), is of intermediate length in Pol λ (Ser463–Gln471) and much longer in Pol μ (His366–Arg389) and TdT (Leu381–Gln402) (**Fig. 3b**). Loop I is well ordered and assumes similar conformations in multiple crystal structures of TdT[27]. In TdT structures, Loop I is positioned within the substrate-binding cleft, occluding binding of a template strand upstream of the active site, and is therefore suggested to be responsible for the strict template independence of TdT[27]. In agreement with this idea, deletion of this loop in Pol μ substantially reduced template-independent activity, favoring template dependence[6,35]. Notably, although Pol μ is capable of template-independent polymerization, it is mainly template dependent. This suggests that Loop I in Pol μ may adopt different conformations depending on the nature of the substrate[6,35]. In agreement with this hypothesis, in our complex with a templated substrate, Loop I (His366–Arg389) is completely disordered (Ala371–Val386) and the DNA duplex is bound in the usual manner within the active site. Thus, the inherent flexibility of this loop in Pol μ is distinct from TdT and suggests how Pol μ can accommodate different substrates.

As for Pol β and Pol λ, the 5′-phosphate of the downstream primer in the gapped DNA is bound by the 8-kDa domain of Pol μ. However, there are fewer interactions than in Pol λ or Pol β, and the binding pocket is not as positively charged (**Fig. 4c**). In polymerases with dRP lyase activity, this pocket contains the proposed lysine nucleophile necessary for dRP lyase activity (Pol β Lys72 and Pol λ Lys312). This residue is a valine (Val212, **Fig. 1b**) in Pol μ, which lacks dRP lyase activity[3]. Therefore, the 8-kDa subdomain of Pol μ is probably conserved for its ability to bind 5′-phosphorylated termini for filling of short gaps and for bridging broken DNA ends during NHEJ. This hypothesis is supported by the observation that polymerase activity of

Pol μ is decreased by approximately 20-fold when the downstream primer is not 5′-phosphorylated[17].

Pol μ and Pol λ can efficiently use substrates containing an unpaired base in the template strand, whereas Pol β cannot[6]. This ability has been suggested to be related to the roles of Pol μ and Pol λ in NHEJ. Perhaps accordingly, in comparison with Pol β, Pol μ and Pol λ have fewer interactions with the template strand near the active site[23] . In addition, Pol μ, in contrast to Pol λ, has fewer interactions with nucleotides T6 and T7, which may not be present in certain NHEJ intermediates lacking a template strand nucleotide opposite the primer terminus[6]. Notably, biochemical data suggest that polymerization on such intermediates can be catalyzed only by Pol μ. This indicates that the observed substrate specificities of these polymerases have a structural basis.

The ability to polymerize on substrates lacking a template strand nucleotide opposite the primer terminus appears to be the defining catalytic property of Pol μ. This unusual reaction seems to partly depend on His329, which structural (**Fig. 6**) and biochemical (**Figs. 7** and **8**) data suggest contributes to stabilizing the primer terminus when the polymerase encounters this type of substrate. As considered earlier[6,35], the data in **Figure 8** do not exclude limited template-independent synthesis by Pol μ during NHEJ. Nonetheless, they confirm the previous suggestion that Pol μ can catalyze template-dependent synthesis from a primer lacking a complementary template base[6], and they indicate that His329 contributes to this mode of synthesis. Thus, this histidine is required whenever the primer and incoming nucleotide cannot be aligned by base-pairing with the template, whether the nucleotide is added randomly or in a manner largely dependent on a template from another DNA end in the context of NHEJ[6] (**Fig. 8c**,**d**).

Comparing the structures of the four mammalian family X DNA polymerases suggests additional experiments that should shed light on the different substrate preferences and biological functions of these polymerases in base excision repair, NHEJ and possibly translesion DNA synthesis and mutagenesis. In a more general sense, the collective efforts on the structural biology of family X polymerases serve as a general paradigm for investigating the biological functions of closely related members of the same polymerase family, whether they are involved in DNA repair (family X), translesion synthesis (for example, family Y) or DNA replication (family B).

METHODS

Expression and purification of the murine Pol μ catalytic core. The coding sequence (residues Pro132–Ala496) of murine Pol μ was cloned into the pGEX-4T3 bacterial expression vector (GE Healthcare) using the EcoRI and XhoI restriction sites, with a tobacco etch virus (TEV) protease cleavage site upstream of the Pol μ coding sequence. The vector was transformed into *Escherichia coli* BL21 Codon-Plus (DE3)-RIL cells. Expression was at 18 °C, induced by adding IPTG to 0.2 mM. Cells were harvested by centrifugation and sonicated in 1× PBS, 500 mM NaCl and 5% (v/v) glycerol. Murine Pol μ was purified by batch incubation of the soluble fraction with glutathione sepharose 4B resin, then cleaved from the resin using TEV protease. The protein was further purified by gel-filtration chromatography over a Superdex75 16/60 column. Peak fractions were pooled and dialyzed into buffer containing 25 mM Tris (pH 8.0), 200 mM NaCl, 5% (v/v) glycerol and 1 mM dithiothreitol (DTT), and the protein was concentrated. Polymerase activity was assayed by primer extension[36]. No exonuclease activity was detected.

Crystallization and data collection. The DNA oligonucleotides used were: 11-nt template (5′-CGGCAACGCAC-3′), 5-nt upstream primer (5′-GTGCG-3′), and 4-nt downstream primer (5′-pGCCG-3′). Oligonucleotides were mixed in equimolar ratios in 100 mM Tris pH 7.5 and 40 mM $MgCl_2$. The DNA was annealed in a thermal cycler by denaturation at 94 °C, followed by a slow temperature gradient from 90 to 4 °C. Hybridized DNA was mixed with Pol μ (3.4:1 DNA/protein ratio) at 4 °C for 1.5 h before adding ddTTP to 0.9 mM. The mixture was incubated at 4 °C for 1 h. Crystals of the ternary complex were formed using the microbatch method[37]. The protein–DNA complex was mixed with an equal volume of crystallization solution (95 mM sodium citrate (pH 5.6), 19% (v/v) isopropanol, 19% (w/v) PEG 4,000 and 5% (v/v) glycerol) and allowed to equilibrate. Crystals reached usable size within 48 h. The crystals were transferred from the original microbatch drop into a sitting-drop tray containing a 1:1 dilution of mother liquor and protein buffer. The crystal reached a cryoprotected state by overnight vapor diffusion. The crystal was frozen in liquid nitrogen and placed into a stream of nitrogen gas cooled to –180 °C for data collection. The data were collected on the Southeast Regional Collaborative Access Team (SER-CAT) 22-ID (or 22-BM) beamline at the Advanced Photon Source, Argonne National Laboratory. The final model comprises protein residues Ala137–Ala496 and all DNA bases, including the incoming ddTTP.

Structure solution. A lower-resolution data set for Pol μ was collected to 2.6 Å on an in-house rotating anode source. These data were indexed, integrated and scaled using HKL2000 (ref. 38). Coordinates from the crystal structure of murine TdT (PDB entry 1JMS; ref. 27) were used to solve the molecular replacement problem, using MOLREP in the CCP4 suite[39,40]. The model for murine Pol μ was built by iterative cycles of model building in O[41] and refinement in CNS[42]. The model of Pol μ from the 2.6-Å structure was refined against the 2.4-Å data set reported here, using the same techniques. Data refinement statistics are listed in **Table 2**. Ramachandran statistics were obtained using MolProbity[43]. All structural figures were generated using Molecule A from the PDB file, using MolScript[44] and Raster3D[45].

Analysis of catalytic activity. Full-length human Pol μ was cloned into pET28a, the H329A mutant was generated using QuikChange mutagenesis (Stratagene), and both proteins were expressed and purified as described[23]. For human TdT, the coding sequence (residues Met1–Ala509) was cloned into pGEX-4T3 using the SalI and NotI restriction sites and the H342A mutant was generated by QuikChange mutagenesis. Vectors were transformed into *E. coli*

Table 2 Data collection and refinement statistics

Data collection	
Space group	*P*2(1)
Cell dimensions	
a, *b*, *c* (Å)	71.208, 96.085, 73.09
α, β, γ (°)	90, 106.549, 90
Resolution (Å)	50–2.4 (2.49–2.40)
R_{sym}	10.6 (50.5)
$I / \sigma I$	16.1 (2.53)
Completeness (%)	99.7 (99.5)
Redundancy	3.5 (3.5)
Refinement	
Resolution (Å)	2.4
No. reflections	36,737
R_{work} / R_{free}	23.2 / 27.8
No. atoms	
Protein	5,231
Ligand/ion	929
Water	183
B-factors	
Protein	57.71
Ligand/ion	51.67
Water	47.29
R.m.s. deviations	
Bond lengths (Å)	0.008
Bond angles (°)	1.3

Values in parentheses are for highest-resolution shell.

BL21 (DE3) Rosetta cells, and expression was performed as above. After cleavage by TEV protease, the protein was purified by chromatography on a Mono S HR 5/5 column. Peak fractions were pooled and dialyzed into 25 mM Tris (pH 8.0), 175 mM NaCl and 5% (v/v) glycerol.

Nonhomologous end-joining assay. Human Ku, the XRCC4–ligase IV (LIV) complex and all end-joining substrates were prepared as described[6,46]. Ku (25 nM), 50 nM X4–LIV, 5 nM DNA substrate and 1 nM Pol μ were incubated for 10 min in 25 mM Tris (pH 7.5), 75 mM NaCl, 72.5 mM KCl, 2 mM DTT, 50 μg ml^{-1} BSA, 0.025% (v/v) Triton X-100, 5% (v/v) glycerol and 0.1 mM EDTA, supplemented with 12.5% (w/v) polyethylene glycol (molecular mass greater than 8 kDa). Ligation was initiated by adding 25 μM each dNTP, 5 mM $MgCl_2$, 0.1 mM ATP and 200 ng supercoiled plasmid competitor. Reaction mixtures were incubated at 37 °C for 4 (**Fig. 8a**) or 30 min (**Fig. 8b**), stopped and deproteinized before analysis using nondenaturing 5% (v/v) PAGE.

End-joining efficiencies were calculated as follows. The amount of each product species, determined by phosphorimaging, was multiplied by the number of ligation events per product species, then divided by the number of substrate units for that product species. The sum of these corrected product amounts was then divided by the total unreacted substrate plus product in the reaction. For synthesis in the absence of joining, 25 nM Ku, 50 nM X4–LIV, DNA substrate and 25 nM Pol μ were preincubated for 10 min as above. Substrates were 0.25 nM of labeled DNA with a TC 3′ overhang mixed with 2.5 nM unlabeled substrate with either a TC 3′ overhang (**Fig. 8c**) or an AG 3′ overhang (**Fig. 8d**). Reactions were performed with 100 μM of each of the four ddNTPs added individually. Products were resolved on 8% (v/v) denaturing PAGE after digestion of reactions with HinfI, focusing on a small 55-nucleotide digestion product containing a TC 3′ overhang.

Steady-state kinetic analysis of nucleotide incorporation. Oligonucleotides T18A2 (5′-ACTGGCCGTCGTTCGATAGTACTCACTGTGATC-3′), P1 (5′-GATCACAGTGAGTAC), DP17 (5′-ATCGAACGACGGCCAGT-3′; 5′-phosphorylated) and T15 were from Oligos Etc. For template-dependent synthesis, ^{32}P 5′ end–labeled P1 was hybridized to DP17 and T18A2 to create a single-nucleotide-gapped substrate. Reactions (20 μl) contained 50 mM Tris (pH 8), 1 mM DTT, 4% (v/v) glycerol, 0.1 mg ml^{-1} BSA, 10 mM $MgCl_2$, 200 nM DNA and either 2.5 nM wild-type Pol μ or 5 nM H329A Pol μ. Reactions were initiated by adding dTTP incubating at 37 °C for 4 min (wild-type Pol μ) or 8 min (H329A Pol μ). For template-independent synthesis, T15 primer was ^{32}P 5′ end–labeled. Reactions (20 μl) contained 50 mM Tris (pH 8), 1 mM DTT, 4% (v/v) glycerol, 0.1 mg ml^{-1} BSA, 0.5 mM $MnCl_2$, 200 nM DNA and either 5 nM wild-type Pol μ or 25 nM H329A Pol μ. Reactions were initiated by adding dTTP and incubating at 37 °C for 8 min. Products were resolved by 16% (v/v) PAGE and quantified by phosphorimagery. The data were fit to the Michaelis-Menten equation using nonlinear regression.

Accession codes. Protein Data Bank: Coordinates have been deposited with accession code 2IHM.

ACKNOWLEDGMENTS

We thank T. Hall and S.Nick McElhinny for critical reading and thoughtful comments on the manuscript. This research was funded in part by the Division of Intramural Research of the National Institute of Environmental Health Sciences, US National Institutes of Health, and in part by US National Institutes of Health grant CA097096 to D.A.R. The Advanced Photon Source used for this study was supported by the US Department of Energy, Office of Science, Office of Basic Energy Sciences, under contract no. W-31-109-Eng-38. We thank Z. Jin for collecting these data at SER-CAT using mail-in crystallography.

AUTHOR CONTRIBUTIONS

A.F.M., cloning, expression and purification of proteins used for biochemistry and crystallography, crystallization of catalytic domain of murine Pol μ; M.G.-D., expression and purification of proteins to be used for biochemical assays, kinetic analysis of human Pol μ and TdT; K.B., analysis of enzymatic activity for human Pol μ and TdT proteins; B.S.D., analysis of end-joining activity for human Pol μ in NHEJ assays; X.Z., early crystallization trials with human Pol μ; D.A.R., analysis of end-joining activity for human Pol μ and interpretation of data from NHEJ assays; L.C.P., analysis of crystallization data and refinement of Pol μ structural model; T.A.K., experimental design and analysis of biochemical data. All authors contributed to experimental design, interpretation of results and preparation of the manuscript.

COMPETING INTERESTS STATEMENT

The authors declare that they have no competing financial interests.

Published online at http://www.nature.com/nsmb/
Reprints and permissions information is available online at http://npg.nature.com/reprintsandpermissions/

1. Bebenek, K. & Kunkel, T.A. Functions of DNA polymerases. *Adv. Protein Chem.* **69**, 137–165 (2004).
2. Braithwaite, E.K. *et al.* DNA polymerase lambda mediates a back-up base excision repair activity in extracts of mouse embryonic fibroblasts. *J. Biol. Chem.* **280**, 18469–18475 (2005).
3. Garcia-Diaz, M., Bebenek, K., Kunkel, T.A. & Blanco, L. Identification of an intrinsic 5′-deoxyribose-5-phosphate lyase activity in human DNA polymerase lambda: a possible role in base excision repair. *J. Biol. Chem.* **276**, 34659–34663 (2001).
4. Fan, W. & Wu, X. DNA polymerase lambda can elongate on DNA substrates mimicking non-homologous end joining and interact with XRCC4-ligase IV complex. *Biochem. Biophys. Res. Commun.* **323**, 1328–1333 (2004).
5. Lee, J.W. *et al.* Implication of DNA polymerase lambda in alignment-based gap filling for nonhomologous DNA end joining in human nuclear extracts. *J. Biol. Chem.* **279**, 805–811 (2004).
6. Nick McElhinny, S.A. *et al.* A gradient of template dependence defines distinct biological roles for family X polymerases in nonhomologous end joining. *Mol. Cell* **19**, 357–366 (2005).
7. Bertocci, B., De Smet, A., Weill, J.C. & Reynaud, C.A. Nonoverlapping functions of DNA polymerases mu, lambda, and terminal deoxynucleotidyltransferase during immunoglobulin V(D)J recombination *in vivo*. *Immunity* **25**, 31–41 (2006).
8. Lieber, M.R. The polymerases for v(d)j recombination. *Immunity* **25**, 7–9 (2006).
9. Bollum, F. Terminal deoxynucleotidyl transferase. *The Enzymes* **10**, 145–171 (1974).
10. Gilfillan, S., Benoist, C. & Mathis, D. Mice lacking terminal deoxynucleotidyltransferase: adult mice with a fetal antigen receptor repertoire. *Immunol. Rev.* **148**, 201–219 (1995).
11. Bertocci, B., De Smet, A., Berek, C., Weill, J.C. & Reynaud, C.A. Immunoglobulin kappa light chain gene rearrangement is impaired in mice deficient for DNA polymerase mu. *Immunity* **19**, 203–211 (2003).
12. Mahajan, K.N., Nick McElhinny, S.A., Mitchell, B.S. & Ramsden, D.A. Association of DNA polymerase mu (Pol mu) with Ku and ligase IV: role for Pol mu in end-joining double-strand break repair. *Mol. Cell. Biol.* **22**, 5194–5202 (2002).
13. Dominguez, O. *et al.* DNA polymerase mu (Pol mu), homologous to TdT, could act as a DNA mutator in eukaryotic cells. *EMBO J.* **19**, 1731–1742 (2000).
14. Zhang, Y., Wu, X., Yuan, F., Xie, Z. & Wang, Z. Highly frequent frameshift DNA synthesis by human DNA polymerase mu. *Mol. Cell. Biol.* **21**, 7995–8006 (2001).
15. Zhang, Y. *et al.* Lesion bypass activities of human DNA polymerase mu. *J. Biol. Chem.* **277**, 44582–44587 (2002).
16. Covo, S., Blanco, L. & Livneh, Z. Lesion bypass by human DNA polymerase mu reveals a template-dependent, sequence-independent nucleotidyl transferase activity. *J. Biol. Chem.* **279**, 859–865 (2004).
17. Nick McElhinny, S.A. & Ramsden, D.A. Polymerase mu is a DNA-directed DNA/RNA polymerase. *Mol. Cell. Biol.* **23**, 2309–2315 (2003).
18. Ruiz, J.F. *et al.* Lack of sugar discrimination by human Pol mu requires a single glycine residue. *Nucleic Acids Res.* **31**, 4441–4449 (2003).
19. Davies, J.F., II, Almassy, R.J., Hostomska, Z., Ferre, R.A. & Hostomsky, Z. 2.3 Å crystal structure of the catalytic domain of DNA polymerase beta. *Cell* **76**, 1123–1133 (1994).
20. Sawaya, M.R., Pelletier, H., Kumar, A., Wilson, S.H. & Kraut, J. Crystal structure of rat DNA polymerase beta: evidence for a common polymerase mechanism. *Science* **264**, 1930–1935 (1994).
21. Pelletier, H., Sawaya, M.R., Wolfle, W., Wilson, S.H. & Kraut, J. Crystal structures of human DNA polymerase beta complexed with DNA: implications for catalytic mechanism, processivity, and fidelity. *Biochemistry* **35**, 12742–12761 (1996).
22. Sawaya, M.R., Prasad, R., Wilson, S.H., Kraut, J. & Pelletier, H. Crystal structures of human DNA polymerase beta complexed with gapped and nicked DNA: evidence for an induced fit mechanism. *Biochemistry* **36**, 11205–11215 (1997).
23. Garcia-Diaz, M. *et al.* A structural solution for the DNA polymerase lambda-dependent repair of DNA gaps with minimal homology. *Mol. Cell* **13**, 561–572 (2004).
24. Garcia-Diaz, M., Bebenek, K., Krahn, J.M., Kunkel, T.A. & Pedersen, L.C. A closed conformation for the Pol lambda catalytic cycle. *Nat. Struct. Mol. Biol.* **12**, 97–98 (2005).
25. Garcia-Diaz, M. *et al.* Structure-function studies of DNA polymerase lambda. *DNA Repair (Amst.)* **4**, 1358–1367 (2005).
26. Garcia-Diaz, M., Bebenek, K., Krahn, J.M., Pedersen, L.C. & Kunkel, T.A. Structural analysis of strand misalignment during DNA synthesis by a human DNA polymerase. *Cell* **124**, 331–342 (2006).
27. Delarue, M. *et al.* Crystal structures of a template-independent DNA polymerase: murine terminal deoxynucleotidyltransferase. *EMBO J.* **21**, 427–439 (2002).

28. Doherty, A.J., Serpell, L.C. & Ponting, C.P. The helix-hairpin-helix DNA-binding motif: a structural basis for non-sequence-specific recognition of DNA. *Nucleic Acids Res.* **24**, 2488–2497 (1996).
29. Osheroff, W.P., Jung, H.K., Beard, W.A., Wilson, S.H. & Kunkel, T.A. The fidelity of DNA polymerase beta during distributive and processive DNA synthesis. *J. Biol. Chem.* **274**, 3642–3650 (1999).
30. Osheroff, W.P., Beard, W.A., Yin, S., Wilson, S.H. & Kunkel, T.A. Minor groove interactions at the DNA polymerase beta active site modulate single-base deletion error rates. *J. Biol. Chem.* **275**, 28033–28038 (2000).
31. Latham, G.J. *et al.* Vertical-scanning mutagenesis of a critical tryptophan in the "minor groove binding track" of HIV-1 reverse transcriptase. *J. Biol. Chem.* **275**, 15025–15033 (2000).
32. Batra, V.K. *et al.* Magnesium induced assembly of a complete DNA polymerase catalytic complex. *Structure* **14**, 757–766 (2006).
33. Beese, L.S. & Steitz, T.A. Structural basis for the 3′-5′ exonuclease activity of *Escherichia coli* DNA polymerase I: a two metal ion mechanism. *EMBO J.* **10**, 25–33 (1991).
34. Gryk, M.R. *et al.* Mapping of the interaction interface of DNA polymerase beta with XRCC1. *Structure* **10**, 1709–1720 (2002).
35. Juarez, R., Ruiz, J.F., McElhinny, S.A., Ramsden, D. & Blanco, L. A specific loop in human DNA polymerase mu allows switching between creative and DNA-instructed synthesis. *Nucleic Acids Res.* **34**, 4572–4582 (2006).
36. Garcia-Diaz, M. *et al.* DNA polymerase lambda, a novel DNA repair enzyme in human cells. *J. Biol. Chem.* **277**, 13184–13191 (2002).
37. Chayen, N.E. Comparative studies of protein crystallization by vapour-diffusion and microbatch techniques. *Acta Crystallogr. D Biol. Crystallogr.* **54**, 8–15 (1998).
38. Otwinowski, Z. & Minor, V. Processing of X-ray diffraction data collected in oscillation mode. *Methods Enzymol.* **276**, 307–326 (1997).
39. Collaborative Computational Project, Number 4. The CCP4 suite: programs for protein crystallography. *Acta Crystallogr. D Biol. Crystallogr.* **50**, 760–763 (1994).
40. Vagin, A. & Teplyakov, A. MOLREP: an automated program for molecular replacement. *J. Appl. Cryst.* **30**, 1022–1025 (1997).
41. Jones, T.A., Zou, J., Cowan, S. & Kjeldgaard, M. Improved methods for building protein models in electron density maps and the location of errors in these models. *Acta Crystallogr. A* **47**, 110–119 (1991).
42. Brunger, A.T. *et al.* Crystallography & NMR system: A new software suite for macromolecular structure determination. *Acta Crystallogr. D Biol. Crystallogr.* **54**, 905–921 (1998).
43. Lovell, S.C. *et al.* Structure validation by Calpha geometry: phi,psi and Cbeta deviation. *Proteins* **50**, 437–450 (2003).
44. Kraulis, P. MOLSCRIPT: a program to produce both detailed and schematic plots of proteins. *J. Appl. Cryst.* **24**, 946–950 (1991).
45. Merritt, E.A. & Murphy, M.E. Raster3D Version 2.0. A program for photorealistic molecular graphics. *Acta Crystallogr. D Biol. Crystallogr.* **50**, 869–873 (1994).
46. Nick McElhinny, S.A., Snowden, C.M., McCarville, J. & Ramsden, D.A. Ku recruits the XRCC4-ligase IV complex to DNA ends. *Mol. Cell. Biol.* **20**, 2996–3003 (2000).

Corrigendum: Structural insight into the substrate specificity of DNA Polymerase μ

Andrea F Moon, Miguel Garcia-Diaz, Katarzyna Bebenek, Bryan J Davis, Xuejun Zhong, Dale A Ramsden, Thomas A Kunkel & Lars C Pedersen

Nat. Struct. Mol. Biol. **14**, 45–53 (2007); **published online 10 December 2006; corrected after print 15 June 2007**

In the version of this article initially published, the crystallization conditions were incorrectly reported. The correct conditions are as follows: 95 mM sodium citrate (pH 5.6), 19% (v/v) isopropanol, 19% (w/v) PEG 4,000 and 5% (v/v) glycerol. The error has been corrected in the HTML and PDF versions of the article. The authors apologize for any inconvenience this may have caused.